Spectral enstrophy budget in a shear-less flow with turbulent/non-turbulent interface

Andrea Cimarelli, Giacomo Cocconi, Bettina Frohnapfel, and Elisabetta De Angelis

Citation: Physics of Fluids **27**, 125106 (2015); doi: 10.1063/1.4937433
View online: http://dx.doi.org/10.1063/1.4937433
View Table of Contents: http://scitation.aip.org/content/aip/journal/pof2/27/12?ver=pdfcov
Published by the AIP Publishing

PHYSICS OF FLUIDS **27**, 125106 (2015)

Spectral enstrophy budget in a shear-less flow with turbulent/non-turbulent interface

Andrea Cimarelli,[1,2] Giacomo Cocconi,[3] Bettina Frohnapfel,[3] and Elisabetta De Angelis[1,4,a)]
[1]*DIN - University of Bologna, Via Fontanelle, 40, 47121 Forlì, Italy*
[2]*DISMI - University of Modena and Reggio Emilia, Via Giovanni Amendola, 2, 42122 Reggio Emilia, Italy*
[3]*ISTM - Karlsruhe Institute of Technology, 76131 Karlsruhe, Germany*
[4]*School of Engineering - Cardiff University, Queen's Buildings, The Parade, Cardiff CF24 3AA, United Kingdom*

(Received 4 February 2015; accepted 13 October 2015; published online 28 December 2015)

A numerical analysis of the interaction between decaying shear free turbulence and quiescent fluid is performed by means of global statistical budgets of enstrophy, both, at the single-point and two point levels. The single-point enstrophy budget allows us to recognize three physically relevant layers: a *bulk turbulent region*, an *inhomogeneous turbulent layer,* and an *interfacial layer*. Within these layers, enstrophy is produced, transferred, and finally destroyed while leading to a propagation of the turbulent front. These processes do not only depend on the position in the flow field but are also strongly scale dependent. In order to tackle this multi-dimensional behaviour of enstrophy in the space of scales and in physical space, we analyse the spectral enstrophy budget equation. The picture consists of an inviscid spatial cascade of enstrophy from large to small scales parallel to the interface moving towards the interface. At the interface, this phenomenon breaks, leaving place to an anisotropic cascade where large scale structures exhibit only a cascade process normal to the interface thus reducing their thickness while retaining their lengths parallel to the interface. The observed behaviour could be relevant for both the theoretical and the modelling approaches to flow with interacting turbulent/nonturbulent regions. The scale properties of the turbulent propagation mechanisms highlight that the inviscid turbulent transport is a large-scale phenomenon. On the contrary, the viscous diffusion, commonly associated with small scale mechanisms, highlights a much richer physics involving small lengths, normal to the interface, but at the same time large scales, parallel to the interface. [http://dx.doi.org/10.1063/1.4937433]

I. INTRODUCTION

Most flows in practical cases are characterized by the coexistence of turbulent and non-turbulent regions. Examples are turbulent jets, turbulent boundary layers, gravity currents, flame fronts, and plumes. In such flows, the dynamics of the turbulent/non-turbulent interface play a very important role since they control relevant flow properties such as mixing rates, heat, and momentum transport.[1] Despite its importance, the understanding of the physics of the interface between turbulent/non-turbulent flows has been recognized as rather elusive. The reason is given by the coupling of the complex multi-scale interactions commonly observed in fully developed turbulent flows with interfacial phenomena which lack a rigorous interpretation and definition.

Since Corrsin and Kistler[2] who provided the first study of interfacial processes, several works have been carried out aiming at understanding the interaction between turbulent/nonturbulent regions. It is well known that at the interface, the fluid in the non-turbulent region is entrained by the

a)Electronic mail: e.deangelis@unibo.it

turbulent flow thus leading to a propagation of the turbulent front. It is believed that entrainment is enforced locally by small-scale turbulent diffusion. A number of experiments and numerical simulations support this thesis by linking some properties of the turbulent/non-turbulent interface to the small scale features of the flow.[3–6] Despite the fact that the interface propagation has an intrinsically viscous origin, it has been shown that at large Reynolds numbers, the entrainment rate and the velocity of propagation are independent of viscosity.[7] Thus, some properties as the mean propagation velocity of the interface or the concentration jumps across the interface have been found to be proportional to the centreline velocity in jets,[4,8] or to the turbulent intensity for oscillating-grid turbulence.[9] This means that despite the work of adding irrotational fluid is thought to act at (viscous) small scale level, the overall rate of entrainment is dictated by the large scale properties of the flow. To reconcile this dual description, it has been argued in Liberzon *et al.*[10] and Sreenivasan *et al.*[11] that the global entrainment flux determined by the mean entrainment velocity u_e and a projected area A_0 can also be characterized in terms of a small-scale local entrainment velocity v_n over a bigger convoluted interface area. The total convoluted surface is thought to adjust together with the local entrainment velocity in such a way that the entrainment flux results to be independent from viscosity; nevertheless, how actually this should happen is not yet clear. Other contradictory results come from the observation of turbulent kinetic energy budgets[12] and enstrophy budget[13] close to the interface, which show weak contributions from viscous diffusion when compared to the advective and production terms. In a recent study on interfaces in jets and zero-mean-shear flows, Wolf *et al.*[14] split the local entrainment velocity in a viscous and in an inviscid contribution $v_n = v_n^{vis} + v_n^{inv}$. By means of conditional averages with respect to the different local shapes of the interface, they find that the local entrainment mechanisms are influenced by the local curvature and the vorticity gradient. Indeed, v_n^{vis} is stronger where the interface has a convex (re-entrant) shape while for concave (protruding) shapes, it acts against entrainment. On the other hand, the inviscid term v_n^{inv} is weaker for convex shape and stronger for the concave ones, but always contributes to the propagation of the interface. They conclude that vortex stretching is the driving term to produce convolution while viscous diffusion tends to flatten the interface.

Most of the studies previously cited focus on local properties of the interface (local geometry, structures topology, local gradients of enstrophy, local propagation velocities) in order to infer on the governing mechanisms of the entrainment process. From a phenomenological point of view, these local and conditional approaches highlight a picture of turbulent entrainment that is composed mainly by two relevant processes: a large-scale inviscid phenomenon usually referred to as engulfment and a small-scale partially viscous mechanism known as nibbling.[4,15] Which mechanism dominates the processes of entrainment and mixing is still debated. The reason is partially due to difficulties in defining quantitatively the processes of nibbling and engulfment thus leading to a rather elusive discrimination of their contribution.

On a different approach, several studies are also devoted to the understanding of other physical aspects such as the mixing spreading, the isotropy recovery, the interface propagation and the structure of small scales. The interaction of two energy-containing turbulence scales in the absence of mean shear is studied in the work of Veeravalli and Warhaft[16,17] where it is found that the mixing layer is strongly intermittent with transverse velocity fluctuations characterized by large skewness. A distinction between intermittent turbulent penetration and turbulent diffusion is made and it is shown that both play an important role in the spreading of the mixing layer. In Tordella *et al.*,[18] the interaction of two isotropic turbulent fields of equal integral scale but different kinetic energy is analysed. Also in this work, intermittency is observed and related with the presence of turbulent energy gradients. This picture is extended in the work of Tordella and Iovieno[19] by analysing how small scale anisotropy and intermittency are generated. It is found that the departure from isotropy is consistent with a reduction of the compression of fluid filaments parallel to the mixing layer and enhancement of the filaments orthogonal to it. Overall, this anisotropy is found to be strongly related with the inhomogeneity induced by the presence of the mixing layer.

Moreover, in general, all the phenomena taking place when turbulent/non-turbulent regions interact are multi-scale mechanisms which strongly depend on the distance from the interface. Indeed, besides the multi-scale feature of turbulence, the presence of the interface induces inhomogeneity thus leading to multi-dimensional physical processes occurring both in the space of scales

and in physical space. Aim of the present work is the analysis of the multidimensional features of the turbulent/non-turbulent interactions. To this end, we study the spectral enstrophy budget equation. This equation allows us to analyse for the first time two distinct transport mechanisms of enstrophy at the basis of the turbulent entrainment. An enstrophy transfers in the space of scales and a spatial flux in the inhomogeneous direction normal to the interface. The clear mathematical distinction of these two transports in diffusive and inertial mechanisms will enable a detailed scale-by-scale analysis of the debated phenomenology of interfacial turbulent/nonturbulent flows. It is worth noting that the formalism of the spectral enstrophy budget equation allows us to give a detailed description of the global statistical features of turbulent flows interfacing with a quiescent laminar region. However, the symmetries of this approach lack the description of the local dynamics of the turbulent interface which would require statistical samples over a convoluted surface. Indeed, in what follows when considering the interface, we will refer to the region of the flow where the interface statistically takes place and not the instantaneous locus of the interface.

The paper is organized as follows. In Section II, we describe the numerical simulations and in Section III, the main properties of the flow are summarized, see the works cited above for a deeper understanding of the flow field. The inhomogeneity of the different regions of the flow is characterized in Section IV by means of the single-point enstrophy budget equation while the multi-dimensionality of the enstrophy production, transport, and destruction is analysed in Section VI by means of the spectral enstrophy budget equation previously introduced in Section V. The paper is finally closed by remarks in Section VII.

II. DIRECT NUMERICAL SIMULATION PROCEDURE

The continuity and Navier-Stokes equations are discretized by means of a pseudo-spectral method based on Fourier series and are integrated in time through a partially implicit Crank-Nicholson/Runge-Kutta scheme, see De Angelis *et al.*[20] for the details on the algorithm. First, a homogeneous isotropic turbulent box with dimensions $2\pi \times 2\pi \times 2\pi$ and discretized by $512 \times 512 \times 512$ Fourier modes is generated through a Gaussian distributed forcing centered at wavenumber $|\mathbf{k}| = 5$ with variance $\sigma = 0.6$. The average Taylor-microscale Reynolds number is $Re_{\lambda 0} = 120$. The Taylor and Kolmogorov length scales are $\lambda_0 = 0.19$ and $\eta_0 = 0.0075$, respectively, while the integral length and time scales are $\ell_0 = 0.4$ and $t_0 = 0.066$, respectively. In this simulation, the spatial resolution is $\Delta x/\eta_0 = 1.6$ and the time step is $\Delta t = 5 \cdot 10^{-5}$. After the steady state is reached, independent velocity fields are sampled to produce the initial conditions for the shear-less turbulent/non-turbulent flow. Indeed, the interfacial flow is generated by matching two identical field of homogeneous isotropic turbulence in a new periodic box with dimensions $4\pi \times 2\pi \times 2\pi$ and $1024 \times 512 \times 512$ Fourier modes and, by means of a continuous function $p(x)$, half of the velocity field is damped to zero. The function

$$p(x) = \frac{1}{2}\left[1 + \tanh\left(a\frac{x}{L}\right)\tanh\left(a\frac{x - L/2}{L}\right)\tanh\left(a\frac{x - L}{L}\right)\right] \tag{1}$$

and the procedure are the same used for the study of shearless mixing in the work of Tordella and Iovieno,[21] Tordella *et al.*,[18] Tordella and Iovieno.[19] From these initial conditions, the flow field is let to freely evolve in time without any forcing. Let us notice that due to the decay of the small scales, the spatial resolution parameter $\Delta x/\eta$ decreases during the simulation. Due to the periodic boundary conditions, the imposed velocity field generates a flow constituted by a homogeneous isotropic turbulent region with two interfaces spreading in opposite directions along the x-direction, see Figure 1(a) to have an idea of the instantaneous topology of the flow across the turbulent/nonturbulent region. In this setting, the y- and z-axes are statistically homogeneous directions. Hence, statistics are obtained by computing spatial averages in the homogeneous (y–z)-planes and ensemble averages over 20 different realizations. The resulting overall average is denoted by angle brackets. In what follows, the results will be shown as a function of the distance from the average position of the interface $X_I = \langle x_I \rangle$, where $x_I = x_I(y, z)$ is the instantaneous position of the interface detected by finding the outermost point where enstrophy, $\Omega = \omega_i\omega_i/2$ with ω_i denoting vorticity, equals a given threshold Ω_{th}. The value of the threshold used for the interface detection is 2% of the mean enstrophy in the turbulent region at a given time t/t_0, i.e., $\Omega_{th} = 0.02\langle\Omega\rangle_{core}$. Though the choice of a given threshold remains arbitrary, the

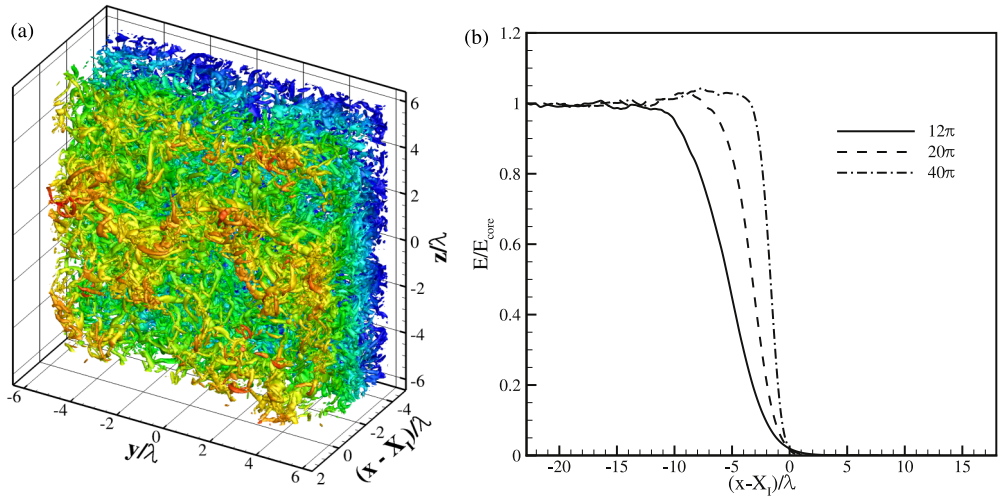

FIG. 1. (a) Topology of the flow across the turbulent/nonturbulent region at $t/t_0 \sim 3$. The isosurfaces denote a specific value of enstrophy, $\Omega \sim 69u_{rms}^2/\lambda^2$, and it is colored by the distance from the mean interface, $(x - X_I)/\lambda$. (b) Initial mean energy profile $E = \langle u_i u_i \rangle/2$ for $a = 12\pi$, $a = 20\pi$, and $a = 40\pi$ normalised by its turbulent core value E_{core}, as a function of the distance from the mean interface.

value adopted here is within a range of values around which the detected interface does not change sensibly with the threshold. The same Ω_{th} is also used in other studies.[7]

Let us finally briefly address the role of the free parameter a of damping function (1). As shown in Figure 1(b), the parameter a determines the initial thickness of the interface region. In particular, by considering Δ as the thickness of the layer in which mean kinetic energy E drops from 75% to 25% of its mean value in the core, E_{core},[18] we have $\Delta = 3.4\lambda_0 = 1.36\ell_0$ for $a = 12\pi$, $\Delta = 2.1\lambda_0 = 0.84\ell_0$ for $a = 20\pi$, and $\Delta = 1.1\lambda_0 = 0.44\ell_0$ for $a = 40\pi$. In the following analysis, the intermediate case $a = 20\pi$ is considered. This value is chosen in order to satisfy two conflicting needs of having an initial interface region large enough to be numerically well resolved and small enough to be considered as an interface, i.e., no larger than an integral length scale ℓ_0, see Ref. 18. However, it is worth noting that the following analysis of the single-point and spectral enstrophy budget has been conducted also for $a = 12\pi$ and $a = 40\pi$. Despite the significant initial topological differences, the main findings presented in the following also hold for these cases.

III. PROPERTIES OF THE FLOW

We report here a general description of the flow field in order to provide instrumental information for the analysis of the following single-point and spectral enstrophy budgets. As already mentioned in Sec. II, from the initial condition, the turbulent/nonturbulent flow is left to freely evolve in time without any forcing, thus leading to a decay. The turbulent kinetic energy decay evaluated in the turbulent core, E_{core}, is shown in Figure 2(a). After an initial transient, the energy decay is found to follow a power law thus suggesting that a self-similar decay[18] takes place for $t/t_0 > 3$. In particular, we measure $E_{core} \sim t^{-1.38}$. During the decay, the Taylor-microscale Reynolds number again evaluated in the core region decreases as shown in Figure 2(b). On the contrary, after a small initial transient, for $t/t_0 > 3$, the Taylor micro-scale evaluated in the turbulent core increases, see the inset of Figure 2(b). Let us point out that in what follows, for the nondimensionalization of lengths and velocities, we will use the time-dependent values of λ and u_{rms} evaluated in the turbulent core. Finally, while decaying, the flow gives rise to a propagation of the turbulent front. As shown in Figure 2(c), the mean interface position propagates as a square-root law of time, $(X_I(t) - X_I(0)) \sim \sqrt{t/t_0}$. This observation actually suggests the possible relevance of local mechanisms of viscous diffusion at the interface.

Overall, we argue that after an initial transient period, the main features of the shear-less turbulent/nonturbulent flow reach a sort of asymptotic behaviour. More precisely, for $t/t_0 > 3$, the energy

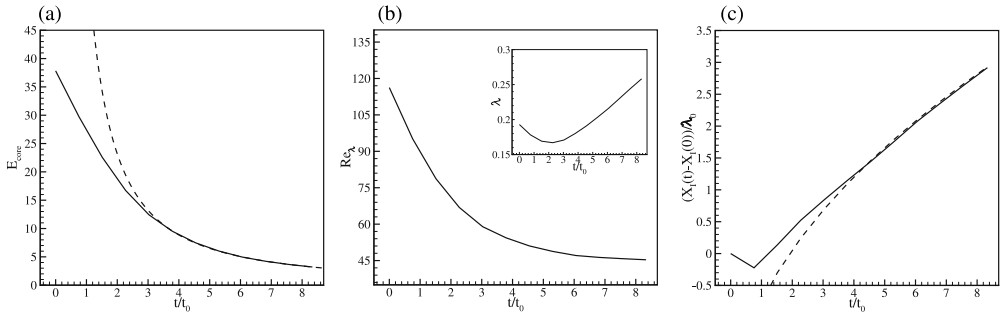

FIG. 2. (a) Time evolution of the turbulent kinetic energy evaluated in the turbulent core, E_{core} (solid line). The dashed line reports the power law $E_{core} \sim t^{-1.38}$. (b) Time behaviour of the Taylor-microscale Reynolds number Re_λ and of the Taylor-microscale λ (inset), both evaluated in the turbulent core. (c) Propagation of the mean interface $(X_I(t) - X_I(0))$ (solid line). The dashed line is a square-root law of time, $(X_I(t) - X_I(0)) \sim \sqrt{t/t_0}$.

decay approaches a self-similar regime by following a power law, $E_{core}(t) \sim t^{-1.38}$, and the Taylor micro-scale increases after a small transient where it is found to decrease. In the following analysis of the single-point and spectral enstrophy budget, we will only discuss results for $t/t_0 = 4.5$. Accordingly to what has been shown, this value is found to be sufficiently far from the initial conditions to reach a sort of asymptotic behaviour, while maintaining at the same time significant values of turbulent energy.

IV. SINGLE-POINT ENSTROPHY BUDGET

We start the analysis of the statistical properties of the shear-less turbulent/non-turbulent flow with the single-point evolution equation of enstrophy. Indeed, as shown in the work of da Silva *et al.*,[1] enstrophy is a very robust and appropriate quantity for the study of interfacial layers between regions of different turbulence intensities. The profile of enstrophy, $\langle\Omega\rangle = \langle\omega_i\omega_i\rangle/2$, where ω_i is the vector field of vorticity, at $t/t_0 = 4.5$ is shown in Figure 3(a), where information about the anisotropy of the flow is also reported by showing the normal and parallel to the interface components of enstrophy, $\langle\omega_x^2\rangle/2$ and $\langle\omega_\pi^2\rangle/2$, respectively, with $\pi = y, z$. Enstrophy is shown to be large and homogeneous well within the turbulent region and to decrease while moving towards the nonturbulent flow. The different components of enstrophy highlight that in the turbulent core, isotropy is maintained while anisotropy appears as we approach the nonturbulent region. In particular, it appears that initially the portion of enstrophy due to the vorticity component parallel to the interface decays faster than that of the normal component, $\langle\omega_\pi^2\rangle/2 < \langle\omega_x^2\rangle/2$. Then, this anisotropy reverses while moving closer and closer to the mean interface where $\langle\omega_\pi^2\rangle/2 > \langle\omega_x^2\rangle/2$. The crossover between these two behaviours takes place at $(x - X_I)/\lambda \sim 4$.

Let us now consider the enstrophy budget equation. Using the symmetries of the present problem, the evolution equation of enstrophy is given by

$$\frac{\partial\langle\Omega\rangle}{\partial t} = \langle\omega_i\omega_j s_{ij}\rangle - \nu\left\langle\frac{\partial\omega_i}{\partial x_j}\frac{\partial\omega_i}{\partial x_j}\right\rangle - \frac{\partial\langle\Omega u\rangle}{\partial x} + \nu\frac{\partial^2\langle\Omega\rangle}{\partial x^2}, \tag{2}$$

where $s_{ij} = 1/2(\partial u_i/\partial x_j + \partial u_j/\partial x_i)$ and $\langle\cdot\rangle$ indicate both the ensemble average and spatial average in the homogeneous $y - z$ planes. Equation (2) allows us to analyse how enstrophy is produced, transferred and destroyed as a function of the distance from the mean interface $(x - X_I)$, see Ref. 13 and for a Lagrangian approach, Refs. 22 and 9. The term on the left-hand side describes how enstrophy decays or increases in time. It is worth noting that since no external forcing is applied to the flow, the overall content of enstrophy decays in time but, depending on the position within the flow, there could be regions where enstrophy increases. Indeed, the inhomogeneity induced by the presence of the interface leads to a spatial redistribution of enstrophy that could contribute to a positive balance of the right-hand side of Equation (2). While the balance of production and destruction of enstrophy, the first and second terms, respectively, is always negative, the action of spatial fluxes could be both positive and negative. The spatial fluxes are driven by two processes,

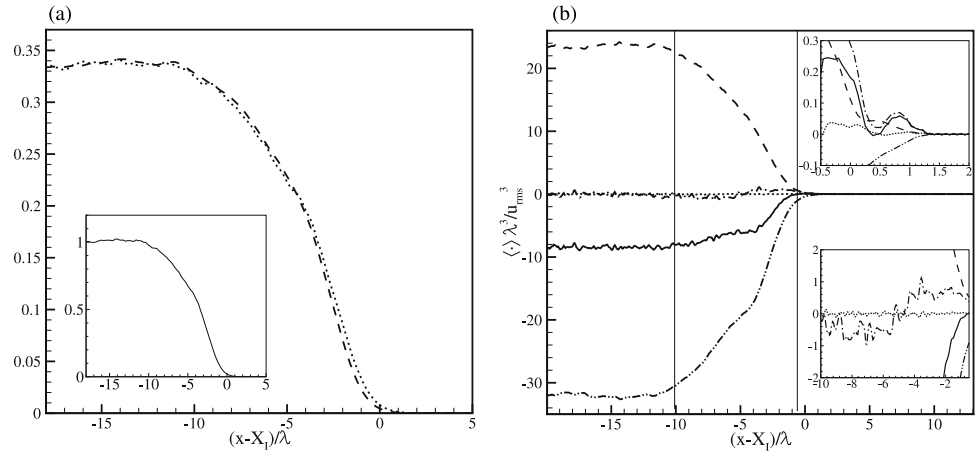

FIG. 3. (a) Averaged profiles of enstrophy $\langle\Omega\rangle$ (inset) and of its parallel and normal to the interface components, $\langle\omega_x^2\rangle/2$ (dashed line) and $\langle\omega_\pi^2\rangle/2$ (dotted line), respectively, normalized with the mean enstrophy at the core, $\langle\Omega_{core}\rangle$, and taken at $t/t_0 = 4.5$ for $a = 20\pi$. (b) Behaviour of the terms of single-point enstrophy budget (2) as a function of the distance from the mean interface position $x - X_I$ for $t/t_0 = 4.5$ and $a = 20\pi$: production (dashed line), destruction (dashed-dotted-dotted line), inertial (dashed-dotted line) and viscous (dotted line) spatial flux, and temporal variation of enstrophy (solid line). The two vertical lines highlight the three relevant regions of the flow. Bottom inset: magnification of the *inhomogeneous layer*. Top inset: magnification of the *interfacial layer*.

one inertial and the other viscous. The first inviscid process is represented by the third term while the viscous diffusion is given by the fourth term.

From this point onward, the terms of the discussed budgets are shown once nondimensionalized with the appropriate quantity formed by using u_{rms} and λ evaluated in the turbulent core at the time considered. The behaviour of the terms of Equation (2) as a function of the distance from the mean interface is shown in Figure 3(b). We distinguish three regions: a *bulk turbulent region*, an *inhomogeneous layer,* and an *interfacial layer*. In the *bulk turbulent region* for $(x - X_I)/\lambda < -10$, enstrophy essentially behaves like a homogeneous isotropic decaying turbulent flow. The effect of the inhomogeneity induced by the presence of the nonturbulent region is very small since the spatial fluxes are negligible. In this region, viscous destruction and production due to vortex stretching are the dominant terms and their negative balance leads to an enstrophy decay. In the *inhomogeneous layer*, for $-10 < (x - X_I)/\lambda < -0.5$, the effect of the presence of the nonturbulent region becomes important. Both, destruction and production of enstrophy decrease while approaching the interface highlighting a strong inhomogeneous feature of this layer. Indeed, the inertial spatial flux is significant. In the inner part of the *inhomogeneous layer* for $-10 < (x - X_I)/\lambda < -5$, enstrophy (while decaying in time) is partially released to feed the regions closer to the non-turbulent flow, $-\partial\langle\Omega u\rangle/\partial x < 0$. The peak of enstrophy drain due to the spatial flux is achieved at $(x - X_I)/\lambda \sim -7$, see the bottom inset of Figure 3(b). In the external part of the *inhomogeneous layer* for $-5 < (x - X_I)/\lambda < -0.5$, the enstrophy decay is lower since the inertial spatial flux changes sign and thus sustains enstrophy, $-\partial\langle\Omega u\rangle/\partial x > 0$. The peak of the enstrophy source due to the spatial flux is reached at $(x - X_I)/\lambda \sim -2$, see the bottom inset of Figure 3(b). As expected, the drain and source behaviour of the spatial fluxes within the *inhomogeneous layer* is essentially driven by inviscid processes while the viscous diffusion is negligible, $|\partial\langle\Omega u\rangle/\partial x| \gg |\nu\partial^2\langle\Omega\rangle/\partial x^2|$. Indeed, the level of turbulence is still high in this layer. In the *interfacial layer* for $(x - X_I)/\lambda > -0.5$, the enstrophy supply of the spatial fluxes compared to the balance between production and destruction is strong enough to give rise to a positive enstrophy variation in time, $\partial\langle\Omega\rangle/\partial t > 0$, see the top inset of Figure 3(b). Although the rate is very small, this is the only region where enstrophy increases in time and corresponds to the layer where the average interface is located. In the *interfacial layer*, the production term is small and the local source of enstrophy is mostly provided by the spatial flux. Also in this region of the flow, this transport of enstrophy is mainly driven by inviscid mechanisms, but for the first time, viscous diffusion starts to play a non-negligible role. It is worth pointing out that the depicted behaviour of the single-point enstrophy budget remains substantially unaltered during all the decay.

A similar behavior is also observed by changing the Reynolds number. Indeed, even if not reported here for brevity, we have also analysed the budget (2) for $t/t_0 = 6$, $t/t_0 = 8$ and for an additional simulation at a lower Reynolds number, $Re_\lambda = 50$. In all these cases, we found that *bulk turbulent region*, the *inhomogeneous layer,* and the *interfacial layer* are roughly located at the same distance $(x - X_I)/\lambda$ from the interface and their role on the enstrophy production, transfer, and dissipation is found to be qualitatively the same.

Overall, we observe that the interactions between turbulent/non-turbulent flow take place mainly in the *inhomogeneous layer* which is 9.5λ wide. These interactions appear to be essentially inviscid and statistically lead to an inertial spatial flux which is responsible for the sustainment of enstrophy at the average position of the interface. It is worth pointing out that the regions where the inertial flux is more intense roughly coincide with the regions of strongest anisotropy between the enstrophy components as shown in Figure 3(a). Thus, it can be thought that the action of turbulent fluctuations advecting enstrophy tends to increase the anisotropy by either drawing the in-plane component of vorticity from the core and transferring it toward the interface or by re-orienting the out of plane vorticity into in-plane direction as suggested by Gampert *et al.*[23] We can conjecture that the peculiar feature of the turbulent fluctuations carrying enstrophy toward the interface may affect the overall behaviour of the turbulent/non-turbulent interface thus leading to different features depending on the turbulent core considered, e.g., boundary layer and jets. Viscosity starts to play a non-negligible role only at the interface by diffusing the level of enstrophy provided there by inviscid mechanisms. Contrary to the *inhomogeneous layer*, the action of viscous diffusion in the external part of the *interfacial layer* should lead to a propagation which is independent on the peculiar feature of the turbulent region, i.e., a more universal behaviour is expected for the interface propagation. Accordingly, in Figure 2(c), we observe a propagation of the turbulent front following the general viscous law, $(X_I(t) - X_I(0))/\lambda \sim \sqrt{t/t_0}$. From the inspection of the data, we measure that the depth of the layer where viscous diffusion overcomes production is $\Delta x = 0.19\lambda = 4.05\eta$. This observation could be consistent with the idea that enstrophy at the outer edge of the interface is diffused by small scales normal to the interface in the order of η. However, at this point, no precise information is available on the scales involved in these processes and could lead to inexact predictions. Indeed, while this conjecture could be true when considering normal to the interface scales, we anticipate here that the analysis of the scale properties of the turbulent/non-turbulent interface through the study of the spectral enstrophy budget that is contained in the rest of the paper actually suggests that the viscous diffusion is a large scale phenomenon in terms of parallel to the interface scales.

In closing this section, let us notice that when studying the local structure of the interface, two adjacent layers bridging the irrotational and turbulent flow are commonly identified, the so-called viscous superlayer and the turbulent sublayer.[1,2,4] These two layers characterize the local dynamic of turbulent entrainment and can be found by means of conditional statistics over convoluted surfaces representing the instantaneous locus of the interface. Contrary to this approach, here, we intend to understand the global statistical features of the entire turbulent flow interacting with a quiescent laminar region without restricting the analysis solely to the interface. In this context, the three regions introduced here represent the simpler way to characterize the inhomogeneity of the flow and, as mentioned in the Introduction, rely on the symmetries of the enstrophy balance equation both at the single-point and two-point levels. Hence, no direct correspondence between the present decomposition and the viscous superlayer and turbulent sublayer can be found since the former characterizes the global features of the entire flow while the latter describe the local dynamics of the interface. However, it is possible to conjecture that the behaviour of the *interfacial layer* is consistent with the presence of a viscous superlayer, in particular in its external part where viscous diffusion overcomes production in a very thin layer whose extension is 4η which is very close to the value of the viscous superlayer thickness reported in the work of Taveira and da Silva.[13]

V. THE BALANCE EQUATION FOR SPECTRAL ENSTROPHY

The description of the turbulent/non-turbulent interactions, made so far in terms of the single-point enstrophy budget, is here extended to a multi-scale framework. Indeed, the mechanisms

of production, transport, and destruction of enstrophy, previously shown, are actually multi-scale phenomena which depend not only on the position with respect to the interface but also on the scale considered. Moreover, it has long been recognized that the dynamics of the interface are linked to two relevant local processes occurring at the interface, the so-called engulfment and nibbling.[1,4,15] By definition, both mechanisms are strongly scale-dependent with engulfment referring to an inviscid large-scale ingestion of non-turbulent fluid, and nibbling referring to a partially viscous process caused by small-scale fluctuations. In this scenario, a compound description in the physical/scale space is required for the correct understanding of the physics of the turbulent entrainment. As an example, in Cimarelli *et al.*,[24,25] the use of a multidimensional approach has been shown to be fundamental for the study and modelling of the energy paths in a turbulent channel flow, while in Philip *et al.*,[5] a multiscale analysis has been successfully applied for the study of the turbulent/non-turbulent interface.

Appropriate candidates to consider for a simultaneous description of dynamics in physical and scale space are the two-point statistical observables, such as the spectral decomposition of enstrophy, $\hat{\Omega} = \hat{\omega}_i \hat{\omega}_i^*/2$, where $\hat{\cdot}$ and * denote the 3D Fourier transform and the complex conjugate, respectively. In the case of homogeneous isotropic turbulence, the balance equation for spectral enstrophy is

$$\frac{\partial \langle \hat{\Omega} \rangle}{\partial t} = -ik_j \langle \hat{\omega}_i^* \widehat{\omega_i u_j} \rangle + \langle \hat{\omega}_i^* \left(\widehat{\omega_j \frac{\partial u_i}{\partial x_j}} \right) \rangle - 2\nu k^2 \langle \hat{\Omega} \rangle, \tag{3}$$

where $k^2 = k_x^2 + k_y^2 + k_z^2$ and i is the imaginary unit. Once considering the turbulent/non-turbulent interface, due to violation of spatial homogeneity, the enstrophy spectrum depends both on the wavenumber considered and on the spatial location. In particular, for the symmetries of the problem, we can derive an evolution equation for the spectral enstrophy written in wavenumber space along the homogeneous (y,z)-directions and in physical space along the inhomogeneous x-direction, i.e., $\tilde{\Omega} = \tilde{\Omega}(x, k_\pi)$, where $\tilde{(\cdot)}$ refers to a 2D Fourier transform in the homogeneous (y–z)-space. The resulting equation reads

$$\frac{\partial \langle \tilde{\Omega} \rangle}{\partial t} = \underbrace{-ik_\pi \langle \tilde{\omega}_i^* \widetilde{\omega_i u_\pi} \rangle}_{T_k} - \underbrace{\langle \tilde{\omega}_i^* \frac{\partial \widetilde{\omega_i u}}{\partial x} \rangle}_{T_x} + \underbrace{\langle \tilde{\omega}_i^* \left(\widetilde{\omega_j \frac{\partial u_i}{\partial x_j}} \right) \rangle}_{\gamma} - \underbrace{2\nu k_\Pi^2 \langle \tilde{\Omega} \rangle}_{\epsilon_k} + \underbrace{\nu \frac{\partial^2 \langle \tilde{\Omega} \rangle}{\partial x^2}}_{D_x} - \underbrace{\nu \langle \frac{\partial \tilde{\omega}_i}{\partial x} \frac{\partial \tilde{\omega}_i^*}{\partial x} \rangle}_{\epsilon_x}, \tag{4}$$

where $k_\pi = k_{y,z}$ and $k_\Pi^2 = k_y^2 + k_z^2$. Equation (4) allows us to analyse the dynamics of enstrophy in the compound wavenumber/physical space. Since the wavenumber space k_π is isotropic, we consider the integral of Equation (4) over a shell in the (k_y, k_z)-space of radius k and thickness dk in order to reduce the degrees of freedom of the analysis. The resulting equation takes the same form as Equation (4) but is a function of a single scalar quantity k and of the position x.

Equation (4) extends the picture delineated with Equation (2) by describing how enstrophy is produced, transferred, and destroyed among different wavenumbers k and distances from the average interface $(x - X_I)$. We can hence have an insight into the scales involved in the viscous and inertial propagation mechanisms of enstrophy in the inhomogeneous x-direction. More explicitly, the term on the left-hand side describes how enstrophy decreases/increases in time as a function of the wavenumber and position considered. This variation in time depends on the local balance between production and viscous destruction and on the amount of enstrophy supply/drain due to the fluxes. The spectral production due to vortex stretching is represented by γ while the effects of viscous destruction are split into two terms: ϵ_k represents the homogeneous viscous destruction related to the in-plane wavenumbers k, while ϵ_x is the viscous destruction associated with the inhomogeneity in the x-direction induced by the presence of the interface. Two kinds of fluxes appear in Equation (4), namely, a spectral flux T_k which identifies the transfer through in-plane wavenumbers k and T_x and D_x which are the inertial and viscous spatial fluxes of spectral enstrophy in the direction normal to the interface, x. It is useful to group together some terms of Equation (4) into an effective source term $\xi = \gamma + \epsilon_k + \epsilon_x$ and into an effective spatial flux $S_x = T_x + D_x$. Hence, the equation for spectral enstrophy reduces to

$$\frac{\partial \langle \tilde{\Omega} \rangle}{\partial t} = \xi + S_x + T_k, \tag{5}$$

allowing to describe in a simple way how for a given wavenumber k and distance from the interface $(x - X_I)$, enstrophy is generated/destroyed (ξ) and transferred through the space of wavenumbers (T_k) and physical space (S_x).

It is worth pointing out that the scales considered here, namely, $2\pi/k$, refer to the lengths of the turbulent structures in the directions parallel to the mean interface. Indeed, the formalism introduced with Equation (4) does not allow us to describe the behaviour of enstrophy in the space of longitudinal scales, $2\pi/k_x$. Nevertheless, Equation (4) contains the contributions from the putative space of longitudinal wavenumbers k_x within the inhomogeneous terms S_x and ϵ_x although in a non-explicit form. This fact increases the complexity of the interpretation of the inhomogeneous terms since we cannot distinguish between mechanisms associated with k_x from those related to the inhomogeneity and hence associated with x-derivatives. In order to explain this point, let us consider to apply Equation (4) to a homogeneous isotropic turbulent flow. With this setting, we may expect that the terms S_x and ϵ_x should vanish since they are conceived as associated with the inhomogeneity of the flow. Actually, these terms will not be zero, even if the term D_x in S_x disappears, since they account also for the spectral flux and viscous destruction among wavenumbers k_x, i.e., for the components $ik_x\langle\hat{\omega}_i^*\widehat{\omega_i u_x}\rangle$ and $2\nu k_x^2\langle\hat{\Omega}\rangle$ of Equation (3) integrated over all wavenumbers k_x. However, let us note that the integral over k of the contribution to S_x coming from $\int ik_x\langle\hat{\omega}_i^*\widehat{\omega_i u_x}\rangle\, dk_x$ is zero for homogeneous isotropic flows, i.e., $\int S_x\, dk = 0$. This information allows us to partially distinguish between inhomogeneous and longitudinal wavenumber effects. Analogously, the integral over k of the contribution to ϵ_x of $\int 2\nu k_x^2\langle\hat{\Omega}\rangle\, dk_x$ is one third of the total viscous destruction for homogeneous isotropic turbulence, i.e., $\int \epsilon_x\, dk = \int \epsilon_k\, dk/2$, and allows us again to discriminate between inhomogeneous and spectral effects.

VI. SPECTRAL ENSTROPHY BUDGETS

Before starting with the analysis of the spectral enstrophy budget equation, let us describe first the behaviour of spectral enstrophy. In Figure 4(a), the logarithm of $\langle\hat{\Omega}\rangle\lambda^3/u_{rms}^2$ is shown as a function of the distance from the mean interface $(x - X_I)/\lambda$ and of the wavenumber $k\lambda$, parallel to the interface, for $t/t_0 = 4.5$. The maximum values of enstrophy are achieved in the *bulk turbulent region* with a peak at small wavenumbers for $k\lambda \sim 2.5$ corresponding to wavelength $\ell/\lambda = 2\pi/(k\lambda) \sim 2.51$. Within the *bulk turbulent region*, the spectral distribution of enstrophy remains unaltered by changing the distance from the mean interface. The dependence on $(x - X_I)/\lambda$ appears in the *inhomogeneous layer* and continues in the *interfacial layer*. In particular, in the inner part of the *inhomogeneous layer* for $-10 < (x - X_I)/\lambda < -5$, the width of the spectral range of enstrophy reduces. Indeed, this is the layer where enstrophy is drained by the spatial flux to feed regions towards the non-turbulent flow. On the contrary, in the external part of the *inhomogeneous*

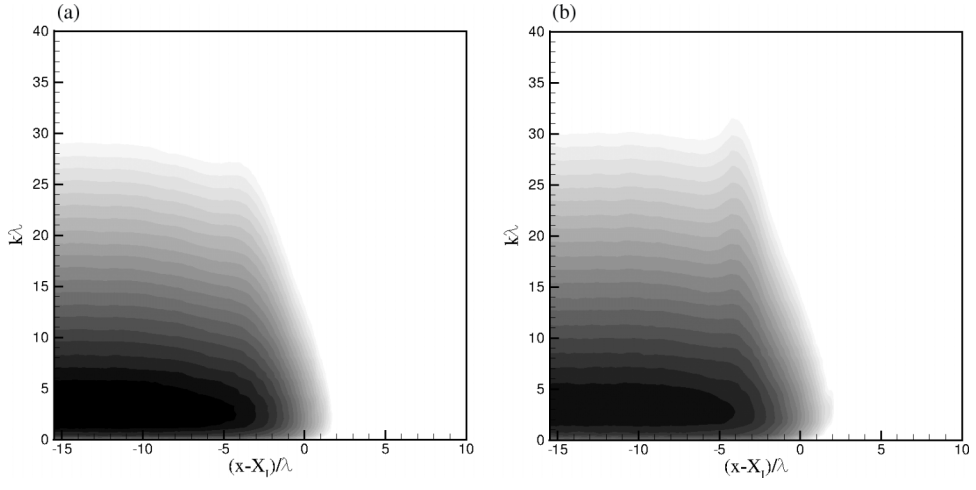

FIG. 4. Isocontours of $\log(\langle\hat{\Omega}\rangle\lambda^3/u_{rms}^2)$ in the $(k, x - X_i)$-space for (a) $t/t_0 = 4.5$ and (b) $t/t_0 = 8$.

layer for $-5 < (x - X_I)/\lambda < -0.5$, the spectral range increases showing a peak. As will be shown in the following, this fact is related to the presence of an enstrophy cascade from large to small scale moving in the interface direction. In the *interfacial layer*, the width of the spectral range of enstrophy decreases. Interestingly, the peak of $\langle\hat{\Omega}\rangle$ remains located, independently of the distance from the mean interface, at $k\lambda \sim 2.5$. As will be shown in the following, the fact that the *interfacial layer* exhibits relatively large parallel to the interface scales is related to the presence of an anisotropic enstrophy cascade. The same observations can be made for $t/t_0 = 8$ as shown in Figure 4(b) where the peak of the spectral width of enstrophy is even more evident. Let us mention at this point that the effect of the Reynolds number has been also analysed by considering an additional simulation at a lower Reynolds, namely, $Re_\lambda = 50$. The same overall features are observed and the effect of Re_λ simply reduces to a shift of the processes at slightly smaller wavenumbers $k\lambda$.

The spectral enstrophy budgets as a function of k are shown in Figures 5–8 for $t/t_0 = 4.5$ and for different distances from the average position of the interface, namely, in the *bulk turbulent region*, in the inner and outer part of the *inhomogeneous layer,* and in the *interfacial layer*. The figures are organized as follows: in plot (a), the compact form of the budget, Equation (5), is shown while in plot (b), the different contributions to the effective source ξ and to the effective spatial flux S_x are reported.

A. The bulk turbulent region

We start the analysis by considering the spectral enstrophy budget within the *bulk turbulent region* shown in Figure 5. We observe that the entire spectrum of scales decays in time. In particular, the rate of decay is larger at relatively small wavenumbers where spectral enstrophy is more intense as shown in Figure 4. In agreement with the picture of a homogeneous isotropic decaying turbulent flow, these enstrophy containing wavenumbers decay in time mostly because of an enstrophy cascade process which drains enstrophy from large structures at small wavenumbers, $T_k < 0$, and releases it to small eddies at larger wavenumbers, $T_k > 0$, where it is destroyed since the source term is negative, $\xi < 0$, due to the action of viscous forces. Actually, the source term shows a positive peak at small wavenumbers since production due to vortex stretching exceeds viscous destruction, $\xi = \gamma + \epsilon_x + \epsilon_k > 0$, but it is not strong enough to balance the flow of enstrophy towards small scales thus leading to a decay. At intermediate wavenumbers, the intensity of spectral enstrophy is smaller. In this range, the source term is negative, $\xi < 0$, and reaches its minimum dissipating the enstrophy available through the cascade process, $T_k > 0$. Since the enstrophy draining due to ξ is larger than the source due to T_k, enstrophy decays also at these wavenumbers.

Due to the statistical homogeneity of this region of the flow, the behaviour of the inhomogeneous terms S_x and ϵ_x has to be understood as a result of spectral interactions in the putative space of longitudinal wavenumbers, k_x. In fact, the integral of S_x is essentially zero, $\int S_x\, dk \sim 0$,

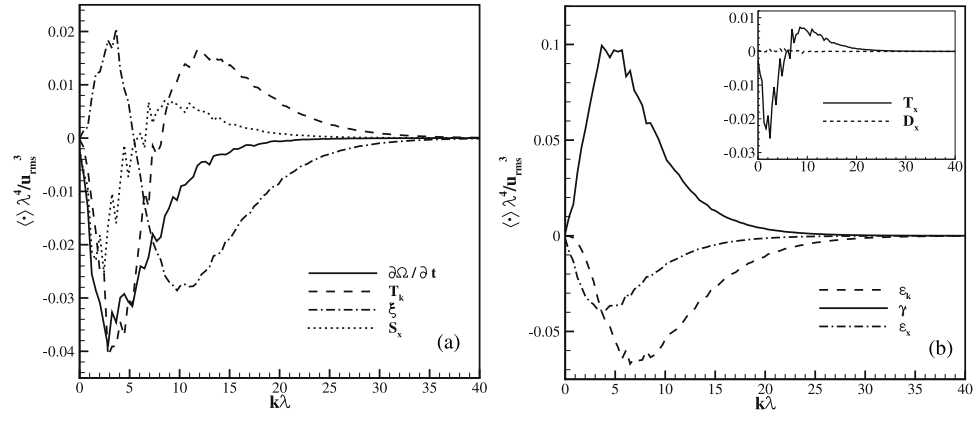

FIG. 5. Spectral enstrophy budget within the *bulk turbulent region* at $(x - X_I)/\lambda = -20$ for $t/t_0 = 4.5$. (a) Spectral behaviour of the different terms of Equation (5). (b) Behaviour of the different components of ξ and of S_x (inset).

highlighting the fact that inhomogeneity and spatial fluxes are negligible in this layer. Hence, the small wavenumber drain and large wavenumber source of S_x appear as the net effect on the space of the wavenumbers k, parallel to the interface, of an enstrophy cascade among the wavenumbers k_x, normal to the interface. Analogously, ϵ_x reports in the k-space the destruction of enstrophy occurring in the putative k_x-space. Indeed, the integral of ϵ_x is roughly half the integral of ϵ_k, i.e., $\int \epsilon_x\, dk \sim \int \epsilon_k\, dk/2$.

Before considering the *inhomogeneous* and *interfacial layers*, it is worth pointing out that in these regions of the flow, the behaviour of these terms is essentially driven by inhomogeneity, thus allowing us to interpret S_x as a spatial flux and ϵ_x as a viscous destruction mainly due to gradients in the x-direction, respectively. Accordingly, the integral of S_x within these regions of the flow is significantly different from zero, $\int S_x\, dk \neq 0$. Hence, the behaviour of S_x is mainly due to the inhomogeneity of the flow and represents a spatial flux of spectral enstrophy which overshadows the scale-by-scale interactions in the putative k_x-space. On the other hand, the integral of ϵ_x is larger than half the integral of ϵ_k, $\int \epsilon_x\, dk > \int \epsilon_k\, dk/2$, highlighting the fact that inhomogeneity introduces an additional viscous destruction related to spatial velocity gradients. The spectral enstrophy budgets in both layers are discussed in Subsections VI B and VI C.

B. The inhomogeneous layer

The spectral enstrophy budget in the inner part of the *inhomogeneous layer* is reported in Figure 6 at $(x - X_I)/\lambda = -7$ where the peak of enstrophy draining of the single-point spatial flux occurs. As highlighted by the single-point enstrophy budget, the inner part of this layer is the region where turbulent/non-turbulent interactions lead to a strong enstrophy release towards the interface, i.e., this is the engine of the turbulent propagation since it is the unique region which significantly releases enstrophy through the spatial flux. As already shown in Figure 4, the overall intensity of spectral enstrophy is reduced in comparison with the *bulk turbulent region* but essentially retains the same spectral distribution, i.e., the enstrophy containing scales are those corresponding to small wavenumbers. As shown in Figure 6(a), analogously to the *bulk turbulent region*, the entire spectrum of enstrophy decays in time. In particular, the decay reaches its maximum at the enstrophy containing scales at small wavenumbers. In this range, the source term is positive, $\xi > 0$, due to vortex stretching mechanisms that are active at the small wavenumber range of this region, see the main plot of Figure 6(b). However, this enstrophy source is not strong enough to balance the small wavenumber enstrophy release due to the spectral flux, $T_k < 0$, and to the spatial flux of enstrophy, $S_x < 0$. These large scales (small wavenumbers) are thus responsible for feeding enstrophy at smaller scales (larger wavenumbers) through a cascade process and to sustain enstrophy in regions closer to the interface through a spatial flux in physical space. Hence, a multidimensional transport

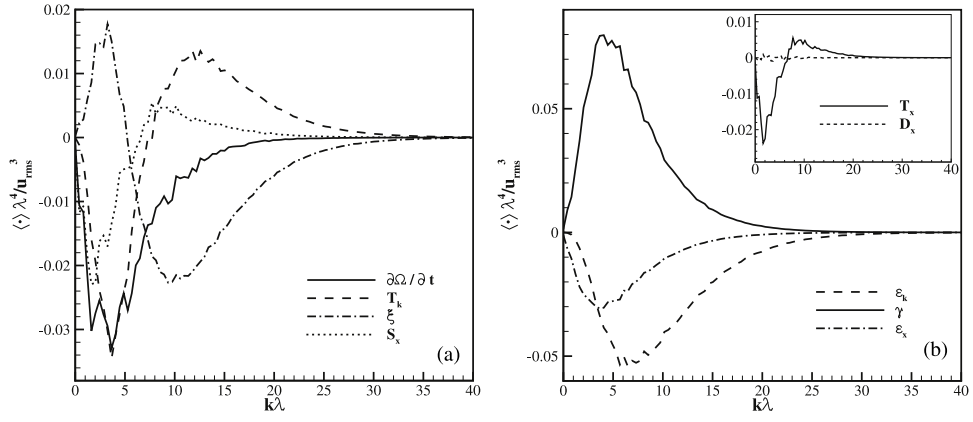

FIG. 6. Spectral enstrophy budget within the *inhomogeneous layer* at $(x - X_I)/\lambda = -7$ where the peak of enstrophy draining due to the spatial flux takes place and for $t/t_0 = 4.5$. (a) Spectral behaviour of the different terms of Equation (5). (b) Behaviour of the different components of ξ and of S_x (inset).

of enstrophy takes place with large scales sustaining a transport of enstrophy towards smaller scales located closer to the interface. In accordance with the single-point budget, the inhomogeneous spatial flux is mainly carried out by inviscid mechanisms, $T_x \gg D_x$, see the inset plot of Figure 6(b). Considering larger wavenumbers, the spatial flux term is essentially negligible and enstrophy is sustained exclusively by the spectral flux, $T_k > 0$. However, this supply of enstrophy is not strong enough to balance the draining of the source term, $\xi < 0$, due to viscous destruction, thus leading to an enstrophy decay also at large wavenumbers.

In the external part of the *inhomogeneous layer* shown in Figure 7, the picture is completely modified. Figure 7 shows the spectral budget at $(x - X_I)/\lambda = -2$ where the peak of enstrophy source of the single-point spatial flux occurs. As shown by the single-point enstrophy budget, the external part of the *inhomogeneous layer* is a region where enstrophy is sustained by a strong spatial flux emerging from the inner part of this layer. Accordingly, the spectral enstrophy budget shows that the entire spectrum of scales gains enstrophy from the spatial flux, $S_x > 0$. This inhomogeneous enstrophy supply compared to the local source term, ξ, is significant and leads to a reduction of the decay rate which is small compared to the one in the *bulk turbulent region* and in the inner part of the *inhomogeneous layer*. The source term in this region of the flow is negative at all wavenumbers, $\xi < 0$. Indeed, the intensity of production due to vortex stretching, γ, is reduced and found to be overcome by viscous destruction, $\epsilon_x + \epsilon_k$, as can be seen in the main plot of Figure 7(b). The inhomogeneous contribution to destruction, ϵ_x, starts to be comparable in magnitude to the spectral one ϵ_k and is found to act at relatively small wavenumbers where the production mechanisms occur. Also in this region, an enstrophy cascade is present which drains enstrophy at small wavenumbers, $T_k < 0$, and releases it at larger ones, $T_k > 0$. It is worth noting that the enstrophy source due to the spatial flux, S_x, is active at wavenumbers larger than those where the spatial flux drains enstrophy in the inner part of the *inhomogeneous layer*. In particular, from Figure 7(a), we observe that the maximum of enstrophy source from the spatial flux occurs at $k\lambda \approx 5$ while the peak of enstrophy sink of the spatial flux shown in Figure 6(a) takes place at $k\lambda \approx 2$. This spectral shift of the scales involved in the spatial flux, S_x, from the inner to the outer part of the *inhomogeneous layer* is in agreement with the previously mentioned directionality of the enstrophy flux both from large to small scales and toward the interface in physical space. More explicitly, the large scales of the inner part of the *inhomogeneous layer* are responsible to sustain enstrophy at smaller scales toward the interface. As shown in the inset plot of Figures 6(b) and 7(b), this spatial transport is essentially an inviscid mechanisms, i.e., $T_x \gg D_x$.

C. The interfacial layer

Let us finally analyse the spectral enstrophy budget in the *interfacial layer* shown in Figure 8 for $(x - X_I)/\lambda = 0$. As shown by the single-point enstrophy budget, this is the region of the flow

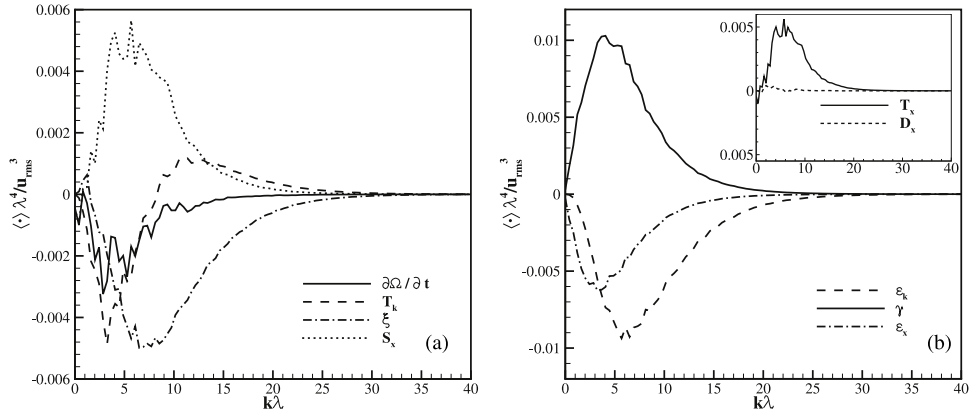

FIG. 7. Spectral enstrophy budget within the *inhomogeneous layer* at $(x - X_I)/\lambda = -2$ where the peak of enstrophy source due to the spatial flux takes place and for $t/t_0 = 4.5$. (a) Spectral behaviour of the different terms of Equation (5). (b) Behaviour of the different components of ξ and of S_x (inset).

where the enstrophy supply due to the spatial flux is strong enough to give rise to a positive variation in time of enstrophy. Furthermore, this is the only region where viscous diffusion is not negligible anymore. Accordingly, the spectral budget in Figure 8(a) shows that enstrophy in the entire spectrum of scales increases in time. As already shown in Figure 4, the enstrophy containing scales is still located at moderately small wavenumbers with a peak of enstrophy at $k\lambda \approx 2.5$. The source term is always negative $\xi < 0$ since production at small wavenumbers, γ, is overcome by an increasingly large viscous destruction associated with the inhomogeneity of this layer, ϵ_x, as shown in the main plot of Figure 8(b). As a consequence, the enstrophy growth is exclusively driven by a strong spatial flux S_x. Interestingly, the peak of enstrophy source due to S_x in the *interfacial layer* is roughly located at the same wavenumber of that in the external part of the *inhomogeneous layer* (both at $k\lambda \approx 5$) as can be seen by comparing Figures 7 and 8. This fact implies that the picture of a double cascade of enstrophy from large to small scales while moving in the interface direction is broken in the *interfacial layer* since the parallel to the interface scales fed by the spatial flux are almost the same. Hence, it appears that in the *interfacial layer,* the turbulent fluctuations while transporting enstrophy towards the non-turbulent region retain their scales parallel to the interface length. This phenomenon can be explained by looking to the behaviour of the spectral transport of enstrophy T_k.

As shown in Figure 8(a), T_k is negative at all wavenumbers. This behaviour may appear anomalous since by the definition of transport term, we may expect a balance between scales gaining and scales losing enstrophy. This peculiar feature is due to the fact that the strong inhomogeneity at the interface induces a significant anisotropy with strong consequences on the cascade mechanisms of enstrophy. The spectral transfer is not anymore isotropic, i.e., directed radially from small to large wavenumbers along the $(\mathbf{k}/|\mathbf{k}|)$-direction. The fact that the entire spectrum of parallel to the interface wavenumbers, k, loses enstrophy in particular at small wavenumbers means that the enstrophy cascade is redirected towards the putative space of longitudinal wavenumbers, k_x, which flows down to small scales up to dissipation. Hence, at the *interfacial layer,* we observe structures with large dimensions parallel to the interface that cascade down reducing their longitudinal thickness while retaining their parallel to the interface lengths. See Figure 9(a) where the instantaneous topology of the flow field is reported, to appreciate the large parallel to the interface surface exhibited by the enstrophy structures.

Let us finally address the role of viscous and inertial mechanisms in the spatial transport of enstrophy in the *interfacial layer*. As shown in the inset plot of Figure 8(b), the viscous contribution to the spatial flux, D_x, is for the first time not negligible. Interestingly, it appears that the wavenumbers gaining enstrophy through a viscous diffusion process are smaller than those gaining from the inviscid transport mechanisms. In particular, the peak of D_x occurs at $k\lambda \approx 2.5$ while the peak of T_x at $k\lambda \approx 5$. This observation may have strong repercussions on the phenomenological understanding of the turbulent/non-turbulent interactions. Indeed, it is commonly assumed that inertial mechanisms are large scale phenomena while viscous mechanisms are small scale processes. In agreement

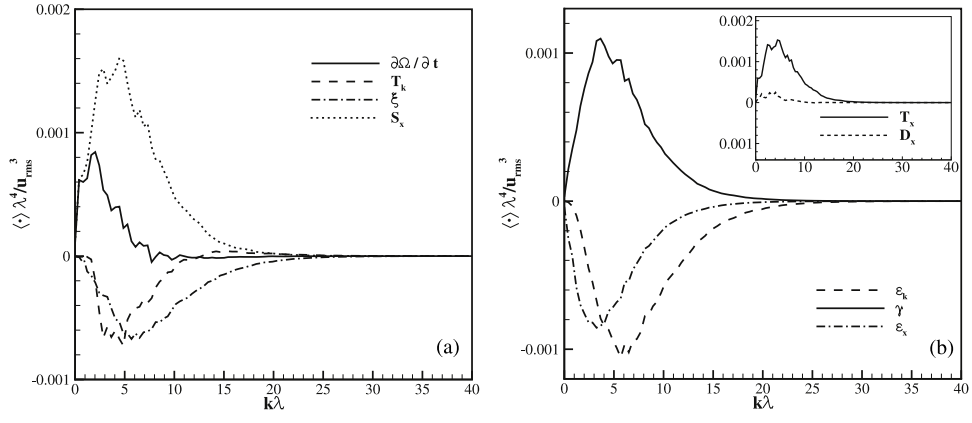

FIG. 8. Spectral enstrophy budget within the *interfacial layer* at $(x - X_I)/\lambda = 0$ for $t/t_0 = 4.5$. (a) Spectral behaviour of the different terms of Equation (5). (b) Behaviour of the different components of ξ and of S_x (inset).

with this picture, we measured in Sec. IV that the thickness of the layer where viscous diffusion is significant is of the order of the Kolmogorov scale, 4η, actually suggesting that the longitudinal length scales involved in the viscous propagation are very small. On the contrary, while considering interface parallel scales, the spectral analysis shows that the viscous diffusion takes place at large scales. This phenomenon is presumably due to the previously shown anisotropic enstrophy cascade at the *interfacial layer* and, hence, with the presence of large structures having very coherent parallel to the interface pattern. Therefore, viscous diffusion acting on top of these fronts is mainly directed along the x-axis leading to a significant contribution to the enstrophy transport at large scales. Accordingly, in Figure 9(b) where the instantaneous enstrophy structures at the interface are colored by the viscous diffusion term, it is shown that the instantaneous contribution of viscous diffusion to the enstrophy transport is mainly active on top of the very coherent and smooth parallel to the interface fronts.

VII. FINAL REMARKS

How turbulent/non-turbulent flows interact leading to a propagation of the turbulent front is analysed here by means of global statistical budgets of enstrophy, both, at the single-point and the two-point levels. Three physically relevant regions are identified for the production, transport, and destruction mechanisms of enstrophy: a *bulk turbulent region*, an *inhomogeneous layer*, and an *interfacial layer*. Enstrophy flows from the *bulk turbulent region* towards the *interfacial layer* by means of inviscid turbulent transport mechanisms. Most of the enstrophy transferred towards the interface is drained by the spatial flux in the inner part of the *inhomogeneous layer* with a peak at seven Taylor microscales behind the average position of the interface. As a consequence, this layer can be considered as the engine of the turbulent front propagation. Most of the enstrophy drained in the inner part of the inhomogeneous layer is then released by the spatial flux in the external part of the *inhomogeneous layer*, two Taylor microscales behind the mean interface. But the *interfacial layer*, where the average position of the interface is located, is the only region where the spatial transport mechanisms are proportionally strong enough to give rise to an enstrophy growth in time. The viscous diffusion is found to be negligible everywhere except in the external part of the *interfacial layer* where it contributes to the transport of enstrophy locally available through inertial mechanisms.

The spectral enstrophy budget shows that enstrophy, while moving towards the non-turbulent region, flows down to smaller scales before being destroyed by viscosity. Hence, larger scales in the inner part of the *inhomogeneous layer* are responsible for feeding enstrophy at smaller scales

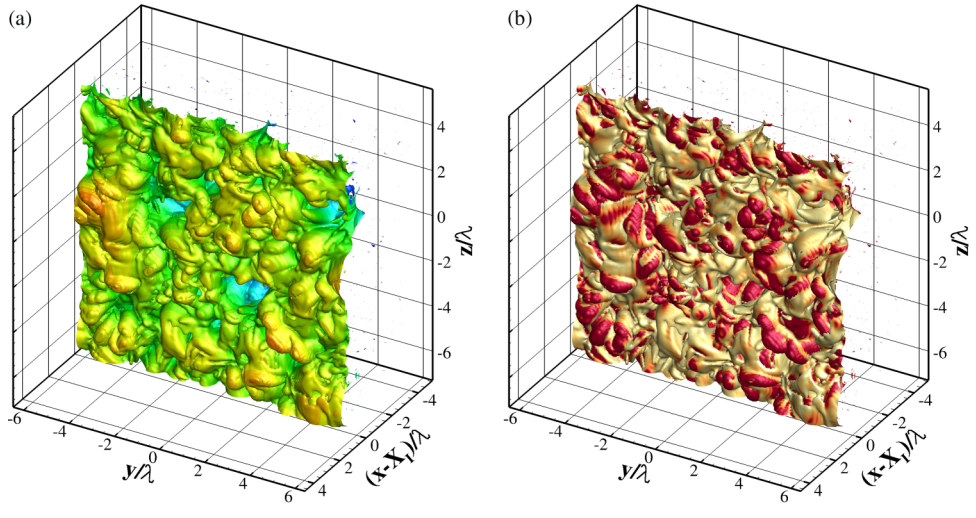

FIG. 9. Instantaneous topology of the turbulent/nonturbulent interface at $t/t_0 = 4.5$. The isosurface denotes the enstrophy threshold, $\Omega = \Omega_{th} = 0.02\langle\Omega_{core}\rangle$, and it is colored by the distance from the mean interface, $(x - X_I)/\lambda$, in (a) and by the viscous diffusion term, $\nu\partial^2\Omega/\partial x^2$, in (b).

in the external part of the *inhomogeneous layer*. This phenomenon is the result of a coupling of an enstrophy cascade in the space of scales with a transport in physical space in the interface direction. Let us point out that this picture of a spatial cascade of enstrophy can be highlighted only through a multidimensional approach. Even if the shift from large to small scales seems to be small, it is important to note that moving along the x-axis, the Kolmogorov scale η is increasing due to a reduction of the local Reynolds number and makes this shift more pronounced than it appears (η is found to double moving from $(x - X_I)/\lambda = -7$ to $(x - X_I)/\lambda = 0$). As a consequence of the combined presence of a cascade process towards small scales and a spatial flux towards the non-turbulent flow, viscous destruction is not anymore an in-plane phenomenon since small scales dissipate enstrophy emerging from larger scales located further away from the interface. This is a peculiar feature of inhomogeneous flows. Once the *interfacial layer* is reached, the symmetries of the enstrophy cascade break down giving rise to an anisotropic cascade where enstrophy does not cascade from large to small parallel to the interface scales but mainly flows down towards small normal to the interface scales where it is then destroyed by viscosity. Hence, in the *interfacial layer*, large parallel to the interface structures experience a reduction of their thickness up to few Kolmogorov scales while essentially retaining their parallel to the interface lengths. This aspect is consistent with the anisotropic structure of the small scales observed in the work of Tordella *et al*.[19] Finally, the transport mechanisms of the spatial cascade of spectral enstrophy are mainly inviscid. Viscosity starts to play a non-negligible role only in the external part of the *interfacial layer*. Interestingly, it is found that the action of viscous diffusion is stronger at scales larger than those where inviscid turbulent mechanisms are dominant. Actually, viscous mechanisms are commonly associated with small scale phenomena. But, as shown here in quantitative terms, viscous diffusion is found to characterize relatively large scales parallel to the interface even if in a very thin layer whose depth is of the order of few Kolmogorov scales. This behaviour is the result of the presence of an anisotropic enstrophy cascade which generates in the *interfacial layer* large parallel to the interface structures characterized by having a very coherent pattern. Hence, viscous diffusion acting on top of these large-scale fronts is mainly directed along the x-axis leading to a significant contribution to the enstrophy transport at large scales. In conclusion, the observed anisotropy of the enstrophy cascade could have strong repercussions on the physical understanding of turbulent/nonturbulent interactions and should be taken into account in the modelling approaches.

In closing this work, let us discuss how the present results on the interactions between shearless turbulent/non-turbulent flows can be generalized to other type of flows. It is shown that inviscid turbulent mechanisms are responsible for carrying enstrophy towards the *interfacial layer*. Most of these complex turbulent/non-turbulent interactions take place in the *inhomogeneous layer*. Through this layer enstrophy is transported by large scale turbulent fluctuations. The main features of these fluctuations are presumably dependent on the turbulent bulk flow that has generated them, and, hence, the main features of the *inhomogeneous layer* are conjectured not to be universal, i.e., they are dependent of the flow considered being either a turbulent jet or boundary layer. According to the fact that vorticity can be transmitted to an irrotational flow only through the tangential forces due to viscosity,[2] in the *interfacial layer*, viscous diffusion is more important and contributes to the transport of enstrophy. Hence, the dynamics of the *interfacial layer* could have a more universal feature since the inertial transport is less important and, above all, far from its source, i.e., the *bulk turbulent region*. Accordingly, the propagation rate of the turbulent front measured here follows a square-root law of time as it is found for all diffusive flows. Overall, these facts suggest that the turbulent region drives the interface through an inertial mechanism while viscosity acts as a final redistribution of enstrophy provided at the interface layer by inertial fluxes.

ACKNOWLEDGMENTS

G.C. and B.F. acknowledge the support through Germany-Israel Foundation for scientific research and development.

[1] C. B. da Silva, J. C. R. Hunt, I. Eames, and J. Westerweel, "Interfacial layers between regions of different turbulence intensity," Annu. Rev. Fluid Mech. **46**, 567–590 (2014).
[2] A. L. Corrsin and S. Kistler, "The free-stream boundaries of turbulent flows," NACA TN-3133, TR-1244, 1955.

[3] M. Holzner, A. Liberzon, B. Lüthi, A. Tsinober, and W. Kinzelbach, "The local entrainment velocity is a viscous quantity," in *Turbulence Heat and Mass Transfer 6 (THMT)*, edited by K. Hanjalić, Y. Nagano, and S. Jakirlić (Begell House, Inc., Rome, 2009).
[4] J. Westerweel, C. Fukushima, J. M. Pedersen, and J. C. R. Hunt, "Momentum and scalar transport at the turbulent/non-turbulent interface of a jet," J. Fluid Mech. **631**, 199–230 (2009).
[5] J. Philip, C. Meneveau, C. M. de Silva, and I. Marusic, "Multiscale analysis of fluxes at the turbulent/non-turbulent interface in high Reynolds number boundary layers," Phys. Fluids **26**, 015105 (2014).
[6] M. van Reeuwijk and M. Holzner, "The turbulence boundary of a temporal jet," J. Fluid Mech. **739**, 254–275 (2014).
[7] M. Wolf, M. Holzner, B. Lüthi, D. Krug, W. Kinzelbach, and A. Tsinober, "Effects of mean shear on the local turbulent entrainment process," J. Fluid Mech. **731**, 95–116 (2013).
[8] B. R. Morton, "Forced plumes," J. Fluid Mech. **5**, 151–163 (1959).
[9] M. Holzner, A. Liberzon, N. Niktin, B. Lüthi, W. Kinzelbach, and A. Tsinober, "A Lagrangian investigation of the small-scale features of turbulent entrainment through particle tracking and direct numerical simulation," J. Fluid Mech. **598**, 465–475 (2008).
[10] A. Liberzon, M. Holzner, B. Lüthi, M. Guala, and W. Kinzelbach, "On turbulent entrainment and dissipation in dilute polymer solutions," Phys. Fluids **21**, 035107 (2009).
[11] K. R. Sreenivasan, R. Ramshankar, and C. Meneveau, "Mixing, entrainment and fractal dimensions of surfaces in turbulent flows," Proc. R. Soc. A **421**, 79–108 (1989).
[12] R. R. Taveira and C. B. da Silva, "Kinetic energy budgets near the turbulent/nonturbulent interface in jets," Phys. Fluids **25**, 015114 (2013).
[13] R. R. Taveira and C. B. da Silva, "Characteristics of the viscous superlayer in shear free turbulence and in planar turbulent jets," Phys. Fluids **26**, 021702 (2014).
[14] M. Wolf, B. Lüthi, M. Holzner, D. Krug, W. Kinzelbach, and A. Tsinober, "Erratum: "Investigations on the local entrainment velocity in a turbulent jet" [Phys. Fluids **24**, 105110 (2012)]," Phys. Fluids **25**, 019901 (2013).
[15] J. Mathew and A. J. Basu, "Some characteristics of entrainment at a cylindrical turbulence boundary," Phys. Fluids **14**, 2065–2072 (2002).
[16] S. Veeravalli and Z. Warhaft, "The shearless turbulence mixing layer," J. Fluid Mech. **207**, 191–229 (1989).
[17] S. Veeravalli and Z. Warhaft, "Thermal dispersion from a line source in the shearless turbulence mixing layer," J. Fluid Mech. **216**, 35–70 (1990).
[18] D. Tordella, M. Iovieno, and P. R. Bailey, "Sufficient condition for Gaussian departure in turbulence," Phys. Rev. E **77**, 016309 (2008).
[19] D. Tordella and M. Iovieno, "Small-scale anisotropy in turbulent shearless mixing," Phys. Rev. Lett. **107**, 194501 (2011).
[20] E. De Angelis, C. M. Casciola, R. Benzi, and R. Piva, "Homogeneous isotropic turbulence in dilute polymers," J. Fluid Mech. **531**, 1–10 (2005).
[21] D. Tordella and M. Iovieno, "Numerical experiments on the intermediate asymptotics of shear-free turbulent transport and diffusion," J. Fluid Mech. **549**, 429–441 (2006).
[22] R. R. Taveira, J. S. Diogo, D. C. Lopes, and C. B. da Silva, "Lagrangian statistics across the turbulent-nonturbulent interface in a turbulent plane jet," Phys. Rev. E **88**, 043001 (2013).
[23] M. Gampert, J. Boschung, F. Hennig, M. Gauding, and N. Peters, "The vorticity versus the scalar criterion for the detection of the turbulent /non-turbulent interface," J. Fluid Mech. **750**, 578–596 (2014).
[24] A. Cimarelli, E. De Angelis, and C. M. Casciola, "Paths of energy in turbulent channel flows," J. Fluid Mech. **715**, 436–451 (2013).
[25] A. Cimarelli and E. De Angelis, "The physics of energy transfer toward improved subgrid-scale models," Phys. Fluids **26**, 055103 (2014).